

Engineering heterostructured Ti<sub>4</sub>O<sub>5</sub>/BaTiO<sub>3</sub> ferroelectric by surface reconstruction for enhanced photocatalytic CO<sub>2</sub> reduction

Ran Su<sup>1#</sup>, Zhitong Sun<sup>1#</sup>, Chao He<sup>1#</sup>, Suna Wei<sup>1</sup>, Lanju Chen<sup>1</sup>, Dawei Zhang<sup>2</sup>, Zhipeng Wang<sup>3\*</sup>, Xingtao An<sup>1\*</sup>, Fa-tang Li<sup>1\*</sup>,

<sup>1</sup>College of Science, Hebei University of Science and Technology, Shijiazhuang 050018, China

<sup>2</sup>School of Materials Science and Engineering, University of New South Wales Australia, Sydney, New South Wales 2052, Australia

<sup>3</sup>Frontier Institute of Science and Technology, State Key Laboratory for Mechanical behavior of Materials, Xi'an Jiaotong University, Xi'an 710049, China

# These authors contributed equally: Ran Su, Zhitong Sun, Chao He.

\* Corresponding authors

[lifatang@126.com](mailto:lifatang@126.com) (F.T. Li); [gstswzp@gmail.com](mailto:gstswzp@gmail.com); [anxt2005@163.com](mailto:anxt2005@163.com)

### Additional Experimental.

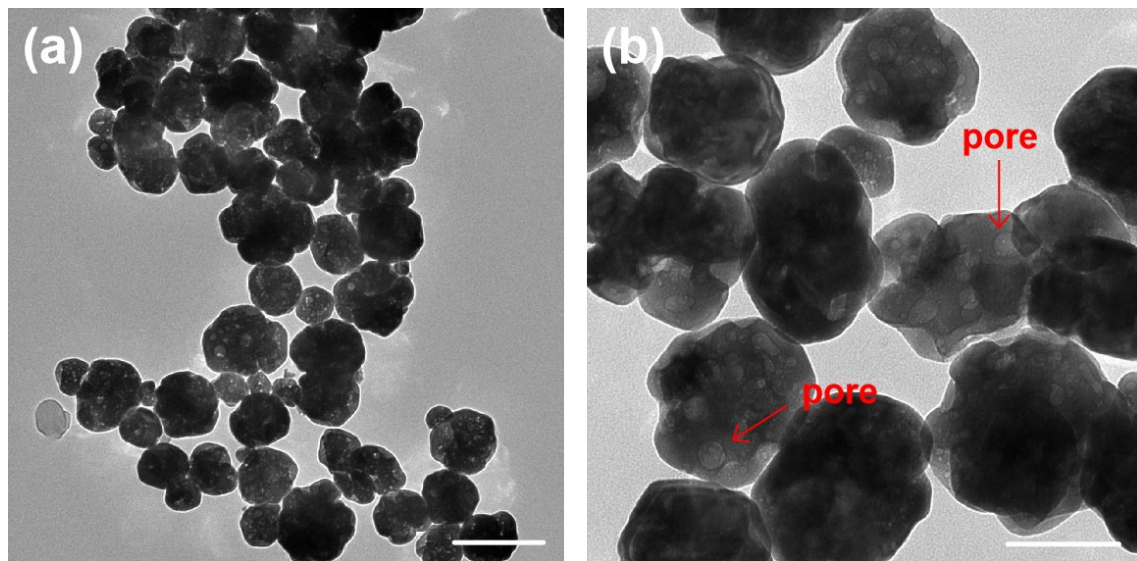


**Fig. S1** TEM image of *b*-BaTiO<sub>3</sub> NPs showing lots of mesopores on the surface of nanoparticles.

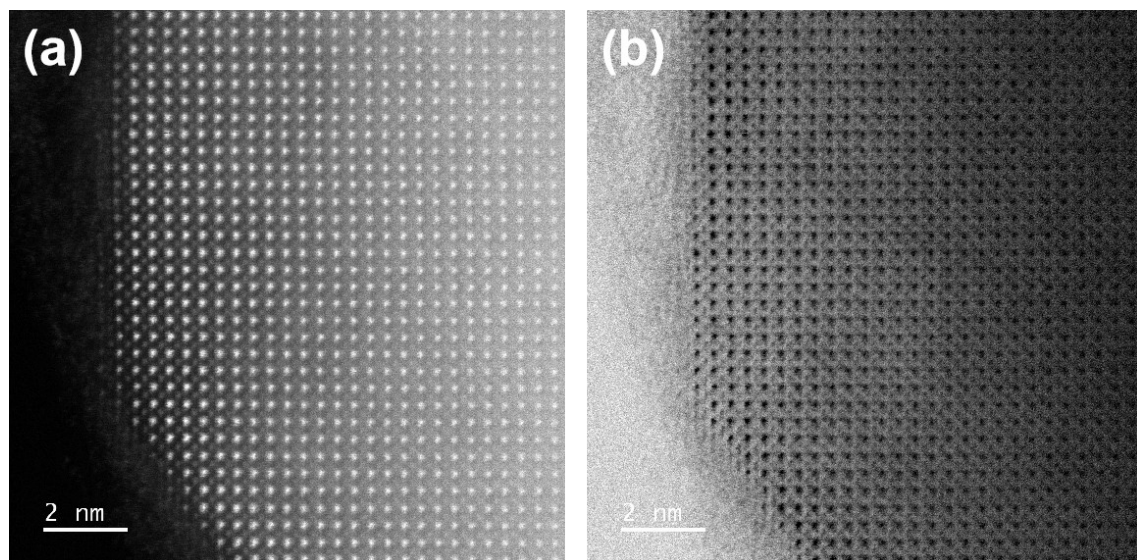


**Fig. S2** HAADF-STEM (a) and HAADF-STEM ABF (b) images of the surface region of pristine BaTiO<sub>3</sub>.

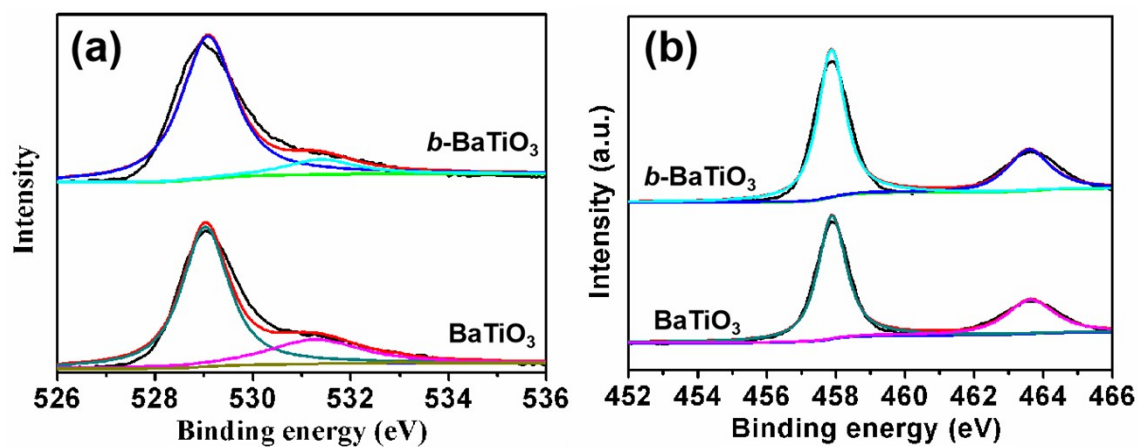


**Fig. S3** O 1s spectra (a) and Ti 2p spectra (b) of the *b*-BaTiO<sub>3</sub> and pristine BaTiO<sub>3</sub>. The XPS data reveal that the pristine BaTiO<sub>3</sub> and *b*-BaTiO<sub>3</sub> show almost no signal from oxygen vacancies and Ti<sup>3+</sup>.

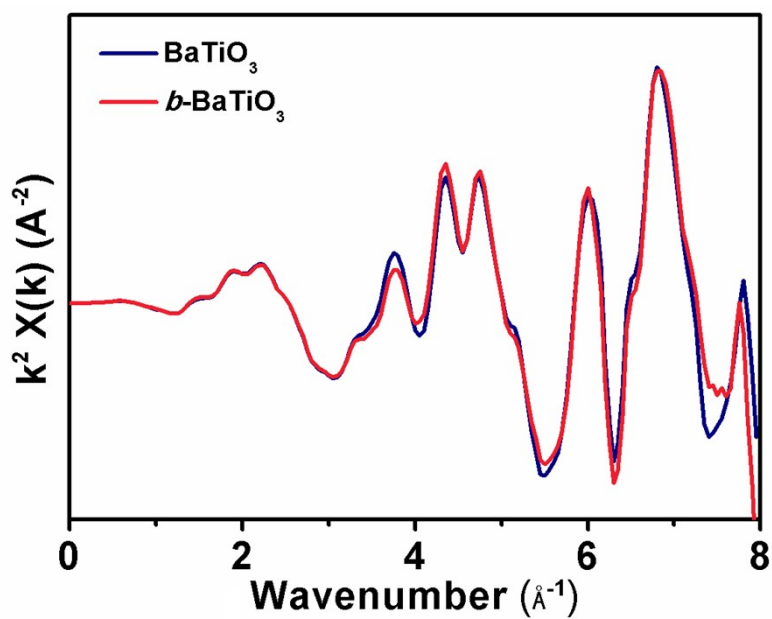


**Fig. S4** Ti K-edge EXAFS oscillation function  $k^2\chi(k)$  for pristine BaTiO<sub>3</sub> and *b*-BaTiO<sub>3</sub>.

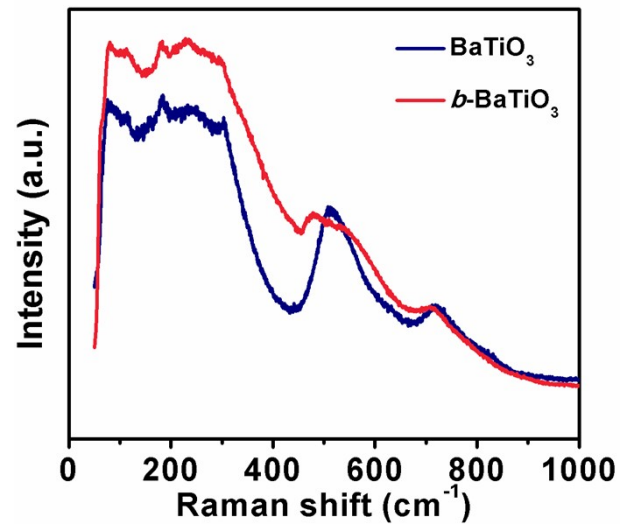


**Fig. S5** Room temperature Raman spectra of the pristine BaTiO<sub>3</sub> NPs and *b*-BaTiO<sub>3</sub>.

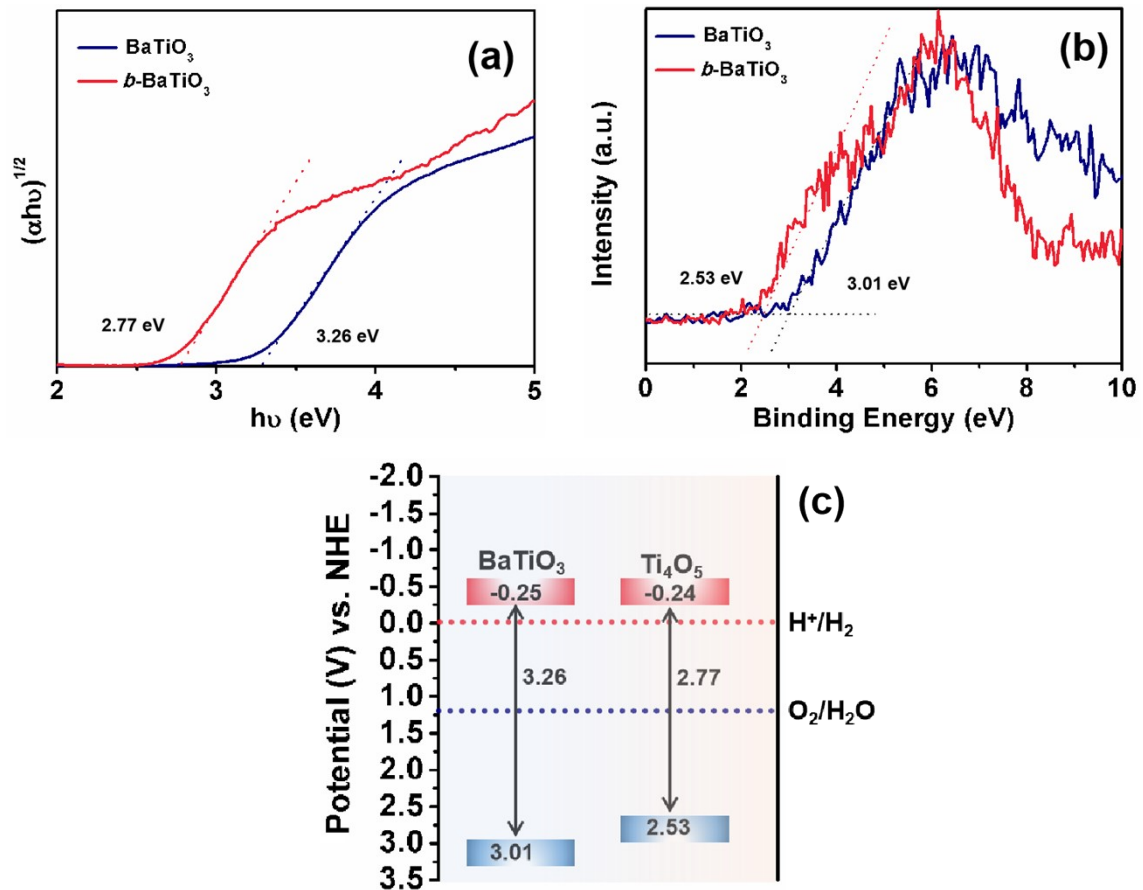


**Fig. S6** (a) Tauc plot of the samples for determining bandgap. (c) Valence band XPS of the pristine BaTiO<sub>3</sub> NPs and *b*-BaTiO<sub>3</sub>. (d) Band energy diagram of *b*-BaTiO<sub>3</sub>.

The band gap ( $E_g$ ) values of the pristine BaTiO<sub>3</sub> and *b*-BaTiO<sub>3</sub> nanoparticles are calculated to be 3.26, and 2.77 eV, respectively. The band gap ( $E_g$ ) value of the pristine BaTiO<sub>3</sub> is equivalent to the BaTiO<sub>3</sub> bulk in ferroelectric heterostructure (*b*-BaTiO<sub>3</sub>). The valence band values are determined to be 3.01 eV and 2.53 eV for the pristine BaTiO<sub>3</sub> and Ti<sub>4</sub>O<sub>5</sub> in *b*-BaTiO<sub>3</sub> nanoparticles, respectively. Based on the UV-vis absorbance and XPS valence band, the positions of the valence band and conduction band of ferroelectric heterostructure (*b*-BaTiO<sub>3</sub>) are presented.

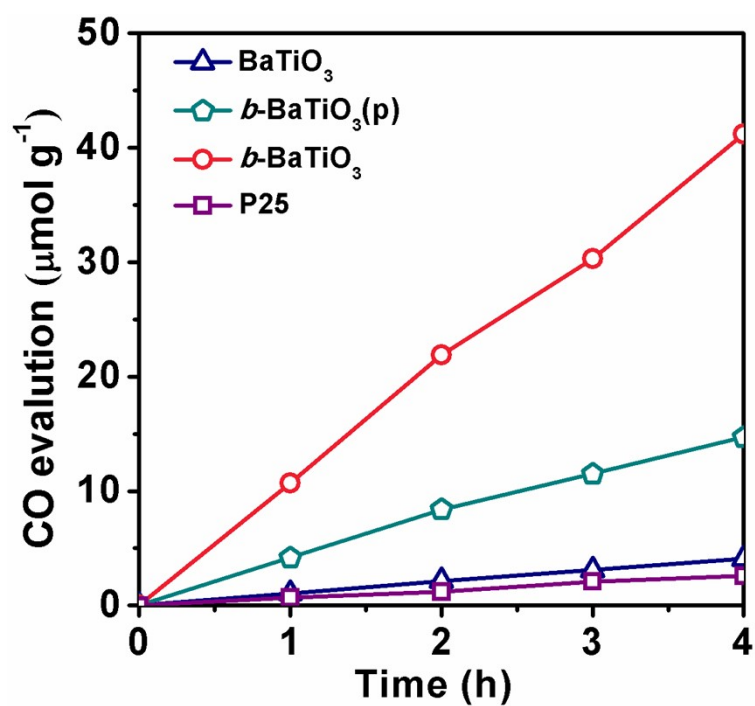


**Fig. S7** Time courses of photocatalytic CO evolutions for BaTiO<sub>3</sub>, *b*-BaTiO<sub>3</sub>(b), BaTiO<sub>3</sub> and P25.

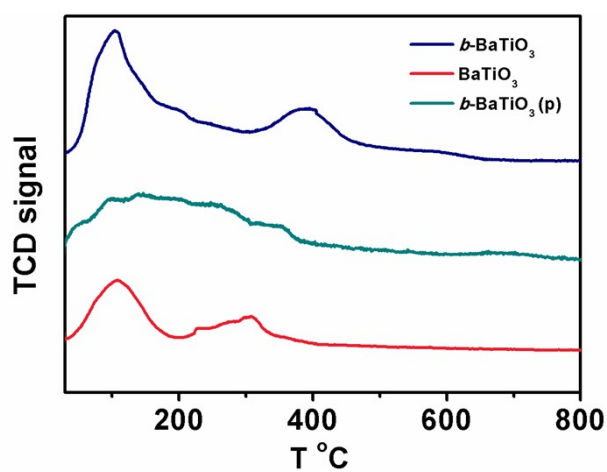


**Fig. S8** CO<sub>2</sub>-TPD profiles of the pristine BaTiO<sub>3</sub>, *b*-BaTiO<sub>3</sub> and *b*-BaTiO<sub>3</sub>(p), respectively.

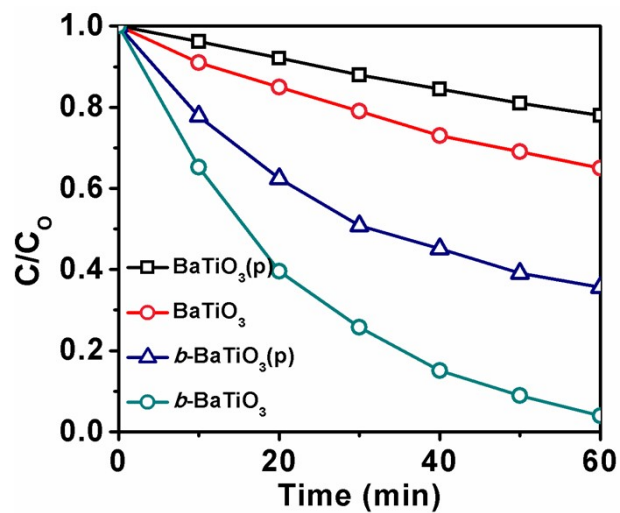


**Fig. S9** Decomposition of Rh B by BaTiO<sub>3</sub>(p) NPs, BaTiO<sub>3</sub> NPs, *b*-BaTiO<sub>3</sub>(p) NPs and *b*-BaTiO<sub>3</sub> NPs, respectively.

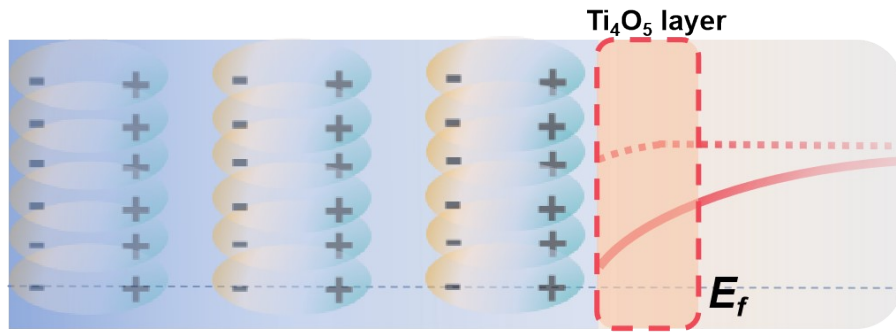


**Fig. S10** Schematic band diagrams of semiconductor/ferroelectric heterojunction.